



# Theoretical investigation of the reactivity of bispentamethylcyclopentadienyl uranium(IV) bithiolate complexes with the heteroallene molecules CS<sub>2</sub> and CO<sub>2</sub>

Fatiha Talbi<sup>a</sup>, Ludovic Castro<sup>b</sup>, Farida Kias<sup>a</sup>, Aziz Elkechai<sup>a,\*</sup>, Abdou Boucekkine<sup>c,\*</sup>, Michel Ephritikhine<sup>d</sup>

<sup>a</sup> Laboratoire de Physique et Chimie Quantique, Faculté des Sciences, Université Mouloud Mammeri de Tizi-Ouzou, 15000, Tizi-Ouzou, Algeria

<sup>b</sup> Université Grenoble Alpes, CNRS UMR 5819, CEA, SyMMES, 38000, Grenoble, France

<sup>c</sup> Univ Rennes, ISCR, UMR 6226 CNRS, Campus de Beaulieu, 35042, Rennes Cedex, France

<sup>d</sup> NIMBE, CEA, CNRS, Université Paris-Saclay, CEA-Saclay, 91191, Gif-sur-Yvette, France

## ARTICLE INFO

### Article history:

Received 30 June 2019

Received in revised form

18 September 2019

Accepted 20 September 2019

Available online 22 September 2019

This paper is dedicated to Dr. Jean-François Halet, CNRS Director of Research at the 'Institut des Sciences Chimiques de Rennes, France', on the occasion of his 60th birthday.

### Keywords:

Bithiolate uranium(IV) complexes

CO<sub>2</sub> and CS<sub>2</sub> activation

Insertion reactions

DFT

Transition state

## ABSTRACT

The insertion reactions of the bispentamethylcyclopentadienyl bithiolate uranium(IV) complexes [U(Cp<sup>\*</sup>)<sub>2</sub>(SR)<sub>2</sub>] (Cp<sup>\*</sup> = η-C<sub>5</sub>Me<sub>5</sub>; R = Me (**1**), <sup>t</sup>Bu (**2**), <sup>i</sup>Pr (**3**), Ph (**4**)) with CO<sub>2</sub> or CS<sub>2</sub> were investigated using Density Functional Theory (DFT), solvent effects being taken into account using the SMD continuum solvation model. The optimized geometries of the bithiolate compounds computed at the DFT/B3PW91 level are in good agreement with available X-ray experimental data. The energy profiles of their reactions with CO<sub>2</sub> and CS<sub>2</sub> were determined. The formation of the products can be explained by a unique reaction mechanism involving an uranium(IV)-bridged heteroallene transition state. The CO<sub>2</sub> insertion reactions exhibit lower activation barriers than those of CS<sub>2</sub> insertion in accordance with the experiments showing that the CO<sub>2</sub> insertion reactions are faster. As expected, compound **2** (R = <sup>t</sup>Bu) was found to be the most difficult to undergo the insertion reaction because of steric hindrance. The geometrical parameters of the CS<sub>2</sub> insertion derivative [U(Cp<sup>\*</sup>)<sub>2</sub>(S<sup>t</sup>Bu)(S<sub>2</sub>CS<sup>t</sup>Bu)] (**5**) and the mixed insertion complex [U(Cp<sup>\*</sup>)<sub>2</sub>(O<sub>2</sub>CS<sup>t</sup>Bu)(S<sub>2</sub>CS<sup>t</sup>Bu)] (**6**) obtained after treatment of **5** with CO<sub>2</sub> are consistent with those determined by X-ray diffraction. The performed orbital analysis reveal the respective role of the actinide 7s, 6d and 5f orbitals, whereas the Wiberg Bond Indices (WBI) afford a good explanation of the structural variations during the insertion reactions. Finally, the Natural Population Analyses account for the different charge transfers occurring during the insertion processes.

© 2019 Elsevier B.V. All rights reserved.

## 1. Introduction

The nuclear waste reprocessing and environmental issues made actinide chemistry a significant field of industrial and academic research. Moreover, the activation of inert small molecules like carbon dioxide CO<sub>2</sub> is an important area investigated these last decades by the chemists who are challenged to develop a new chemistry, known as 'green-chemistry'. Among investigated issues, the transformation of hydrocarbons, as alkanes, by the means of the activation of the C–H bond, the design of new approaches to store

or transform usefully CO<sub>2</sub>, the removal of polluting gases such CFCs through C–F bond activation as well as the use of renewable sources of CH<sub>4</sub> in various industrial sectors [1–4].

Considering uranium complexes, the insertion reactions of the U–E bonds (E = C, F, H, N, O, Se) have been extensively studied, in particular for the complexes carrying the ubiquitous cyclopentadienyl ring and its derivatives [5], and this has resulted in a large variety of actinide complexes with interesting structural features, coordination environments, and reactivity [6–18]. Thus, in order to understand the mechanistic processes involved in these reactions and the role of different ligands coordinated to the metal center, the reactivity of uranium complexes towards CO<sub>2</sub> and CS<sub>2</sub> have been explored theoretically by Ding [19] and co-workers, who demonstrated that the functionalization of CO<sub>2</sub> or CS<sub>2</sub> when dealing with the [U(Tp<sup>\*</sup>)<sub>2</sub>(CH<sub>2</sub>Ph)] (Tp<sup>\*</sup> = hydrotris(3,5-dimethylpyrazolyl)

\* Corresponding author.

\*\* Corresponding author.

E-mail addresses: [azizelkechai@yahoo.fr](mailto:azizelkechai@yahoo.fr) (A. Elkechai), [abdou.boucekkine@univ-rennes1.fr](mailto:abdou.boucekkine@univ-rennes1.fr) (A. Boucekkine).

borate) uranium complex proceeds in a two steps process; the insertion of these small molecules into the U–C bond takes place during the first step and is followed by the reorientation of the PhCH<sub>2</sub>CE<sub>2</sub> (E = O, S) fragment to give the final products. Also, Castro et al. treated the reactivity of the uranium(III) compound [U(MeC<sub>5</sub>H<sub>4</sub>)<sub>3</sub>] [20] with CS<sub>2</sub>, COS, PhN<sub>3</sub> and PhNCO using DFT computations and the B3PW91 functional, and could explain the difference in reactivity between CS<sub>2</sub> and COS, and between PhN<sub>3</sub> and PhNCO. Recently, Cloke et al. investigated experimentally the reductive activation of CO<sub>2</sub> using the mixed–ligand U(III) compound [U(Cp\*)(p–Me<sub>2</sub>bp)] (p–Me<sub>2</sub>bp = C<sub>6</sub>H<sub>4</sub>{p–C(CH<sub>3</sub>)<sub>2</sub>C<sub>6</sub>H<sub>2</sub>Me<sub>2</sub>O<sup>–</sup>})<sub>2</sub>) [21], exhibiting an η<sup>6</sup> interaction with the uranium center, which gave the dinuclear uranium carbonate complex, [U(Cp\*)(p–Me<sub>2</sub>bp)]<sub>2</sub>(μ–η<sup>1</sup>:η<sup>2</sup>–CO<sub>3</sub>).

On the contrary, very little attention was devoted to the M–S metal–sulfur bonds; their discovery in 1982, in the active site of the metalloproteinase [22] boosted the chemistry of the thiolate and sulfide complexes of transition metals which were appreciated for their uses in bioinorganic chemistry, in the study of the nitrogenases [23], and in some industrial processes like oil desulfurization [24]. The actinide thiolate complexes have been practically ignored for a long time, certainly because the U–S bond between a hard metal and a soft atom was reputed to be unstable. Ten years later, this assertion proved to be false with in particular the synthesis and/or the characterization of some thiolate actinide compounds, [U(HBpz<sub>3</sub>)<sub>2</sub>(S<sup>i</sup>Pr)<sub>2</sub>] (pz = pyrazolyl) [25], [Th(Cp\*)(S<sup>i</sup>Pr)<sub>2</sub>] [26], [Li(dme)]<sub>4</sub>[U(SCH<sub>2</sub>CH<sub>2</sub>S)<sub>4</sub>] [27], [U(MeC<sub>5</sub>H<sub>4</sub>)<sub>3</sub>(S<sup>i</sup>Pr)], [U(Me<sub>3</sub>CC<sub>5</sub>H<sub>4</sub>)<sub>3</sub>(SPh)] and [U(Me<sub>3</sub>CC<sub>5</sub>H<sub>4</sub>)<sub>2</sub>(μ–SPh)]<sub>2</sub> [28], [U(N(SiMe<sub>3</sub>)<sub>2</sub>)<sub>3</sub>(S–2,6–Me<sub>2</sub>C<sub>6</sub>H<sub>3</sub>)] [29] and more recently [U(Tp\*)<sub>2</sub>X] (X = CCPh, CCSiMe<sub>3</sub>, NHPH, NHCH<sub>2</sub>Ph, SPh) [30]. These syntheses show that uranium exhibits a strong affinity for sulfur. Generally, the studies of these thiolate complexes were limited to structural investigations, like those reported by Ephritikhine et al. on the monocyclooctatetraenyl and triscyclopentadienyl complexes [U(Cot)(SR)<sub>2</sub>] (Cot = η–C<sub>8</sub>H<sub>8</sub>) [31a] and [U(C<sub>5</sub>H<sub>4</sub>R')<sub>3</sub>(SR)] (R' = H, <sup>t</sup>Bu, SiMe<sub>3</sub>) [31b]. The first reactivity studies on [U(Cp)<sub>3</sub>(S<sup>i</sup>Pr)] (Cp = η–C<sub>5</sub>H<sub>5</sub>) showed that the thiolate ligand could undergo substitution reactions and that unsaturated molecules could be inserted into the U–S bond [32]. In particular, treatment of [U(Cp)<sub>3</sub>(S<sup>i</sup>Pr)] with carbon dioxide led to the formation of [U(Cp)<sub>3</sub>(O<sub>2</sub>CS<sup>i</sup>Pr)], the first compound resulting from the insertion of CO<sub>2</sub> into a metal–sulfur bond [31b], even if this complex could not be isolated in a pure form because of the facile reverse decarboxylation reaction. However, concerning the uranium(IV) species, especially the complexes involving U–S bonds, the theoretical study of the CO<sub>2</sub> and CS<sub>2</sub> insertion into these bonds has not been developed and the understanding of the reaction mechanism not yet completely clarified. So, with the aim of probing various aspects of the reactivity of uranium(IV) thiolate complexes towards small molecules as CO<sub>2</sub> and CS<sub>2</sub>, we found interesting to investigate theoretically the insertion process of these molecules into the U–S bonds of the bithiolate compounds [U(Cp\*)<sub>2</sub>(SR)<sub>2</sub>] [32], which can be considered as models in organo-uranium chemistry [33].

Here, we present a detailed DFT study of the reactivity of a series of bispentamethyl–cyclopentadienylbithiolate uranium(IV) complexes, *i.e.* [U(Cp\*)<sub>2</sub>(SMe)<sub>2</sub>] (**1**), [U(Cp\*)<sub>2</sub>(S<sup>t</sup>Bu)<sub>2</sub>] (**2**), [U(Cp\*)<sub>2</sub>(S<sup>i</sup>Pr)<sub>2</sub>] (**3**) and [U(Cp\*)<sub>2</sub>(SPh)<sub>2</sub>] (**4**) (Fig. 1) towards small heteroallene molecules. The aim is to compare the insertion reactions of CO<sub>2</sub> and CS<sub>2</sub> into actinide–sulfur bonds and to explain their distinct behavior. Indeed, it was found experimentally that the insertion of CO<sub>2</sub> into the U–S bond of the thiolate complexes is easier and faster than that of CS<sub>2</sub>. In particular, we shall investigate what are the electronic and steric factors of the SR thiolate ligands which drive this insertion reactivity of the U(IV) complexes under consideration. The reaction profiles of the reaction will be determined. Moreover, to yield further insight into the interactions between

uranium and small molecules, key features of the electronic and geometric structures will be explored; in particular Wiberg Bond Indices (WBI) [34] and the Natural Population Analysis (NPA) [35] will be used to characterize the bonding and electronic structure of the considered species, during the reaction paths.

## 2. Computational details

Calculations were performed with the Gaussian 09 suite of programs [36]. Density Functional Theory (DFT) was applied by the mean of the B3PW91 hybrid functional [37,38]. In order to treat the actinide center in a suitable way and to greatly reduce computational cost of calculations, two possible relativistic RECP pseudopotentials can be used: the first one where 5f electrons are included in the large–core RECP, and the second one, when active 5f electrons must be described explicitly, being the small–core RECP. According to these considerations, Castro et al. developed two kinds of potentials in relativistic effective core to describe suitably the metal actinide: *i.e.* small–core Stuttgart–Dresden RECP [39] (which includes 1s, 2s, 2p, 3s, 3p, and 3d electrons) and large–core Stuttgart–Dresden RECP [40] (which includes in addition, 4s, 4p, 4d, and 4f electrons) depending on the size of the system.

In the case of actinide U(IV) complexes it has been shown that the large–core RECPs can be used for uranium instead of small–core ones with no less of accuracy (and a shorter computational time) [39]. The RECPs were used in combination with their optimized valence basis sets supplemented by an f polarization function for the large–core RECP used for uranium. The small–core Stuttgart–Dresden relativistic effective core potential [41] was employed for sulfur atoms in association with its valence basis set and an additional d–polarization function [42], while the 6–31 + G(d, p) double zeta basis set was used for the treatment of carbon, oxygen and hydrogen atoms [43]. All geometry optimizations were first carried out without any symmetry constraint considering the whole molecular systems in the gas phase. The solvent effects have been taken into account by a self-consistent reaction field technique using the Solvation Model Density (SMD) continuum model [44] which considers the charge density of the solute interacting with the solvent considered as a dielectric medium. The solvents considered in our computations are those used in the experimental work of Ephritikhine and al. [32], *i.e.* tetrahydrofuran (THF) and toluene.

Several studies have shown that the B3PW91 approach reproduces the experimental geometries and ground state properties of f–element compounds with a satisfying accuracy [45–50] in other words, that the theoretical results are found close to those determined experimentally.

All obtained stationary points located on the PES were characterized as extrema which could be minima (adducts, intermediate states with a number of imaginary frequencies  $N_{\text{imag}} = 0$ ) or first order transition states ( $N_{\text{imag}} = 1$ ) through harmonic approximation vibration frequency calculations. The zero–point vibrational energy (ZPVE) corrections within the harmonic approximation were calculated and included in all reported relative energies given in kcal.mol<sup>–1</sup>, obtained for a temperature of 298.15 K. The Intrinsic Reaction Coordinate (IRC) method [51] was used to confirm the transition states linking the two corresponding minima (adducts, intermediates states or final products). In order to simulate the effects of solvent used in the insertion reactions, we carried out "single–point" calculations with the SMD continuum solvation model [52] implemented in Gaussian 09 software.

Spin–orbit corrections to the energies of the reactants and all other states, *i.e.* adducts, transition states, products, have not been considered, since their effects should be similar for all species during the reaction processes reminding that the latter do not

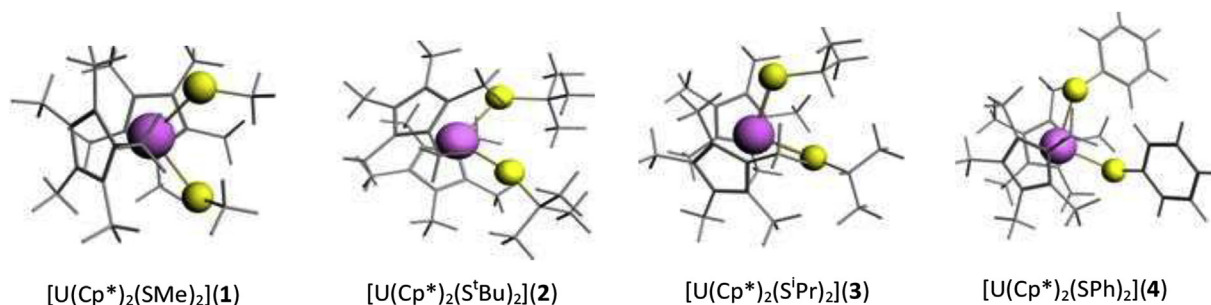


Fig. 1. Studied bis(thiolate) uranium(IV) complexes.

involve any change in the oxidation state of the metal, and therefore will not affect the reaction profile. Indeed, these corrections, mainly of atomic nature [53,54] namely not very sensitive to the environment of the metal ion for a given oxidation state, have a little effect on the computed geometries of actinide molecular compounds and on chemical reactions energies differences [55,56]. It should be noted that in our case, spin contamination, which can occur in DFT calculations since the used unrestricted determinant could exhibit an unwanted mixing of different spin states, was found negligible, owing to the fact that the computed values  $\langle S^2 \rangle$  of the squared spin operator are very close to the exact  $S(S+1)$  values for all the studied species (deviation less than 1%).

The bonding in molecules is often described using the classical chemical ideas of covalency (bond multiplicity) and ionicity (atomic charges). The Wiberg bond order is a measure of electron population overlap between two atoms; using orthonormalized basis functions, it is not calculated the same way as in the Mulliken population analysis (MPA) [57]. For typical chemical bonds, usefully the Wiberg bond order value is generally close to the formal bond order. Besides, the charges derived from the Natural population analysis (NPA) are also more chemically meaningful than MPA charges because they are less basis-set dependent.

### 3. Results and discussion

#### 3.1. Structural properties

First, the full geometry optimizations of the neutral complexes,  $[\text{UCp}^*_2(\text{SMe})_2]$  (**1**),  $[\text{UCp}^*_2(\text{S}^t\text{Bu})_2]$  (**2**),  $[\text{UCp}^*_2(\text{S}^i\text{Pr})_2]$  (**3**) and  $[\text{UCp}^*_2(\text{SPh})_2]$  (**4**), were carried out in the gas phase, at the

unrestricted DFT level of theory using both the hybrid functionals B3PW91 and B3LYP. For all the U(IV)  $5f^2$  complexes, we considered the lowest spin state, i.e. the singlet one which, according to our calculation, corresponds to the ground state. In Table 1 are listed the most relevant computed geometrical parameters, i.e. metal–ligand lengths and bond angles for the studied complexes in the gas phase, and in solution for complex **1** at the DFT/B3PW91 level (the optimized structures and coordinates are given in Supporting Information). Our discussion will be focused first on the optimized geometries obtained for the isolated molecules. As expected, in all the studied molecules, the uranium center is found in a classical pseudo–tetrahedral bent sandwich configuration. The computed U–S bond lengths of all thiolate complexes vary from 2.69 to 2.75 Å and are similar to those observed in other neutral thiolate compounds.

Thus, the U–S bond lengths of complex **1**, namely 2.710 Å as computed at the B3PW91 level, are slightly larger than those measured by X–ray crystallography, 2.639 Å in  $[\text{U}(\text{Cp}^*)_2(\text{SMe})_2]$ , when using the large–core RECP pseudopotential for uranium metal. The same trend for the other lengths of U–Ct and U–C is observed. For example, for complex **1**, displayed on Fig. 2, the carbon atoms of the cyclopentadienyl ring are coplanar; the distance between the uranium atom and the centroid of the  $\text{Cp}^*$  cycle is equal to 2.53 Å in average and is slightly larger than the value of 2.47 Å determined by X–ray crystallography, whereas those between the metal and carbon atoms of the cycle U– $\text{C}_{(\text{Cp})}$  are in average equal to 2.79 Å (values in the gas phase), larger than the experimental values by 0.06 Å. On the other hand, the computed angles correctly reproduce those observed in the crystal; as an example, the angles  $\text{S}_1\text{–U–Ct}_1$  and  $\text{Ct}_1\text{–U–Ct}_2$  of 108.2 and 135.0°

Table 1

Selected Bond Lengths (Å) and Angles (deg) for Compounds 1–4 Computed at the B3PW91 and B3LYP (in parentheses) Levels in the Gas Phase (in Solution, Solely for the Complex 1 in THF with B3PW91 Functional, in Bold; X-ray Values in Italics) [20a].

Complexes				
Geo. Param. <sup>a</sup>	$[\text{U}(\text{Cp}^*)_2(\text{SMe})_2]$ ( <b>1</b> )	$[\text{U}(\text{Cp}^*)_2(\text{S}^t\text{Bu})_2]$ ( <b>2</b> )	$[\text{U}(\text{Cp}^*)_2(\text{S}^i\text{Pr})_2]$ ( <b>3</b> )	$[\text{U}(\text{Cp}^*)_2(\text{SPh})_2]$ ( <b>4</b> )
U–S <sub>1</sub>	2.710 <b>2.738</b> (2.730) 2.639	2.717 (2.709)	2.712 (2.724)	2.732 (2.752)
U–Ct <sub>1</sub>	2.521 <b>2.535</b> (2.560) 2.470	2.546 (2.570)	2.531 (2.558)	2.515 (2.543)
S <sub>1</sub> –C <sub>1</sub>	1.846 <b>1.847</b> (1.859) 1.810	1.884 (1.901)	1.868 (1.878)	1.792 (1.800)
S <sub>1</sub> –U–Ct <sub>1</sub>	108.2 <b>109.5</b> (108.4) 108.4	106.9 (107.7)	111.6 (112.2)	111.226 (111.275)
Ct <sub>1</sub> –U–Ct <sub>2</sub>	135.0 <b>135.7</b> (134.5) 137.6	131.0 (131.2)	134.2 (132.9)	134.6 (133.9)
S <sub>1</sub> –U–S <sub>2</sub>	98.7 <b>87.7</b> (94.1) 97.2	106.9 (87.7)	103.0 (102.7)	103.2 (102.680)
$\langle \text{U–C}_{(\text{Cp})} \rangle$	2.790 <b>2.81</b> (2.793) 2.73	2.810 (2.843)	2.794 (2.832)	2.792 (2.820)

<sup>a</sup> Ct<sub>1</sub> and Ct<sub>2</sub> are the Cp\* ring centroids.

are very close to the X-ray values which are equal to 108.4 and 137.6°, respectively. Finally, as it can be seen in Table 1, the influence of the THF solvent on the optimized geometrical parameters of complex **1** is rather small, even if we note that the U–C<sub>1</sub> and U–S lengths increase slightly in solvent. This result makes us confident that the gas phase optimized geometries are accurate enough for all complexes. The optimized coordinates of all compounds are given in the Supporting Information (Tables S11) whereas the optimized geometries of [U(Cp\*)<sub>2</sub>(SR)<sub>2</sub>] (R = Me, <sup>t</sup>Bu, <sup>i</sup>Pr, Ph) are depicted on Figure S12.

We consider now the Wiberg Bond Indices, which are useful tools for the analysis of bonding and of the electronic structure of organometallic complexes. Generally, the calculated WBI correlate very well with experimental data like bond lengths and vibrational frequencies. In Table 2 are reported the WBI of the U–S and S–C bonds and their corresponding lengths computed at the B3PW91 level in the gas phase.

As it can be seen, the bithiolate uranium complexes exhibit single U–S and S–C bonds with bond indexes close to 1. The U–S bonds which are involved in the insertion reaction, exhibit bond indexes lower than 1, varying from 0.857 for R = Ph to 0.928 for R = <sup>t</sup>Bu. Identical index orders are observed in all cases for the U–S<sub>1</sub> and U–S<sub>2</sub> bonds, in accordance with the similarity of the U–S<sub>1</sub> and U–S<sub>2</sub> bond lengths. The same observation is noticed in the case of the S<sub>1</sub>–C<sub>1</sub> and S<sub>2</sub>–C<sub>2</sub> bonds.

Populations analyses of the thiolate uranium(IV) complexes bring light into some other aspects of the metal–ligands interaction. Despite its well known limitations, because of the strong basis-set dependence and the inconsistency of the results when dealing with non-covalent bond as in the case of some metallic complexes, MPA permits generally to describe qualitatively the evolution of charge transfers and bonding interactions occurring in a series of homologous molecular systems, while the NPA analysis, which has been shown to be useful in inorganic chemistry, provides more reliable atomic net charges. In Table 3 are collected the computed MPA and NPA charges of U, X atoms and Cp\* ligands of the neutral compounds. By net charges of SR and Cp\*, one understands the global charge of the thiolate and the pentamethylcyclopentadienyl ligands respectively, and not only that of the atom connected to uranium.

The Mulliken analysis (detailed in SI) indicates that the MPA net charges (not the real charges) of the metal are largely smaller than its oxidation state +4 for the neutral compounds due to the ligands–to–metal donation, the latter effect being highlighted by the weak negative charges carried by the Cp\* and thiolate ligands.

**Table 2**  
WBI of the U–S and S–C Bonds and their Corresponding U–S and S–C Bond Lengths (Values in Parentheses).

Complex	U–S <sub>1</sub>	U–S <sub>2</sub>	S <sub>1</sub> –C <sub>1</sub>	S <sub>2</sub> –C <sub>2</sub>
[U(Cp*) <sub>2</sub> (SMe) <sub>2</sub> ]	0.903 (2.710)	0.903 (2.710)	1.004 (1.846)	1.005 (1.846)
[U(Cp*) <sub>2</sub> (S <sup>t</sup> Bu) <sub>2</sub> ]	0.928 (2.717)	0.928 (2.719)	0.939 (1.884)	0.939 (1.884)
[U(Cp*) <sub>2</sub> (S <sup>i</sup> Pr) <sub>2</sub> ]	0.915 (2.712)	0.916 (2.714)	0.962 (1.868)	0.963 (1.865)
[U(Cp*) <sub>2</sub> (SPh) <sub>2</sub> ]	0.857 (2.732)	0.856 (2.732)	1.043 (1.792)	1.044 (1.790)

**Table 3**  
MPA and NPA charges from B3PW91 computations in THF.

Complex	MPA/NPA charges				
	U	SR1	SR2	Cp*1	Cp*2
[U(Cp*) <sub>2</sub> (SMe) <sub>2</sub> ]	1.028/1.893	–0.351/–0.428	–0.352/–0.429	–0.164/–0.519	–0.160/–0.517
[U(Cp*) <sub>2</sub> (S <sup>t</sup> Bu) <sub>2</sub> ]	1.042/1.853	–0.365/–0.420	–0.380/–0.432	–0.156/–0.502	–0.142/–0.499
[U(Cp*) <sub>2</sub> (S <sup>i</sup> Pr) <sub>2</sub> ]	1.018/1.870	–0.354/–0.431	–0.356/–0.431	–0.159/–0.504	–0.149/–0.504
[U(Cp*) <sub>2</sub> (SPh) <sub>2</sub> ]	0.993/1.899	–0.368/–0.448	–0.368/–0.451	–0.128/–0.501	–0.129/–0.499

The NPA analysis is supposed to exhibit improved numerical stability and to better describe the electron distribution in molecular systems containing metal atoms compared to the other schemes. As already noticed with MPA, the ligands–to–metal donation is strong for the U(IV) ion; this is highlighted by the decrease of the MPA net charges of the ligands. However, the SR ligands exhibit relatively large negative MPA charge compared to the Cp\* ligand and this negative charge is mainly concentrated on the S atom with a mean value of –0.368 indicating that, despite the covalent aspect of the bonding between the uranium atom and the ligand, the interaction between the uranium and sulfur atoms is more electrostatic in nature than that between U and Cp\* which carry MPA charges of 1.020 and –0.151, respectively. However, according to the NPA analysis, these two electrostatic interactions are of the same order of magnitude. Despite this contradiction, these two charge analyses (MPA and NPA) highlight the electrostatic interaction between the uranium atom and the different ligands. The frontier molecular orbitals (FMO), which are of importance when investigating chemical bonding and reactivity, are now considered. The highest occupied molecular orbital (HOMO) and lowest unoccupied molecular orbital (LUMO) of [U(Cp\*)<sub>2</sub>(SMe)<sub>2</sub>] (**1**) and [U(Cp\*)<sub>2</sub>(S<sup>t</sup>Bu)<sub>2</sub>] (**2**) are displayed in Figure S13. As we note from this figure, the HOMO is composed mainly by the p orbitals of S and C atoms, the contribution of the metal center being negligible, whereas in the LUMO the metal center contributes mainly with the 6d orbitals.

### 3.2. Reactivity of the bithiolate uranium(IV) complexes [U(Cp\*)<sub>2</sub>(SR)<sub>2</sub>] towards CS<sub>2</sub> and CO<sub>2</sub>

The reactivity of the bithiolate uranium(IV) complexes [U(Cp\*)<sub>2</sub>(SR)<sub>2</sub>] (R = Me, <sup>t</sup>Bu, <sup>i</sup>Pr, Ph) with CO<sub>2</sub> and CS<sub>2</sub> is explored using the methodology described below. All obtained stationary points have been fully optimized and were characterized by their frequency using vibrational frequency calculations as minima without any imaginary frequency for ground states, or transition states (TS) with only one imaginary frequency. The IRC calculations confirmed that the found transition states do link the two corresponding minima (of reactants and products).

Experimentally [32], these reactions gave the insertion derivatives [U(Cp\*)<sub>2</sub>(SR)(E<sub>2</sub>CSR)] (E = O and R = <sup>t</sup>Bu; E = S and R = Me, <sup>i</sup>Pr or <sup>t</sup>Bu) where the molecule CS<sub>2</sub> or CO<sub>2</sub> is inserted into the U–S bond of the reactant complexes. [U(Cp\*)<sub>2</sub>(SMe)<sub>2</sub>] reacted with CO<sub>2</sub> in THF under mild conditions (1 atm, 20 °C) to form several unidentified products whereas [U(Cp\*)<sub>2</sub>(S<sup>t</sup>Bu)<sub>2</sub>] reacted very quickly (a few minutes) with CO<sub>2</sub> under the same conditions to form the insertion derivative [U(Cp\*)<sub>2</sub>(O<sub>2</sub>CS<sup>t</sup>Bu)<sub>2</sub>]. Otherwise [U(Cp\*)<sub>2</sub>(SMe)<sub>2</sub>] reacted with CS<sub>2</sub> in toluene to form after a few hours at 70 °C the mono-insertion product [U(Cp\*)<sub>2</sub>(SMe)(S<sub>2</sub>CSMe)]. On the other hand, two days were required to form [U(Cp\*)<sub>2</sub>(S<sup>t</sup>Bu)(S<sub>2</sub>CS<sup>t</sup>Bu)] from [U(Cp\*)<sub>2</sub>(S<sup>t</sup>Bu)<sub>2</sub>].

The simple functionalization of CS<sub>2</sub> or CO<sub>2</sub> through the [U(Cp\*)<sub>2</sub>(SR)<sub>2</sub>] (R = Me, <sup>t</sup>Bu, <sup>i</sup>Pr, Ph) complexes should proceed in a similar way according to Fig. 2 where the reactions of [U(Cp\*)<sub>2</sub>(SMe)<sub>2</sub>] and CO<sub>2</sub> or CS<sub>2</sub> are depicted.

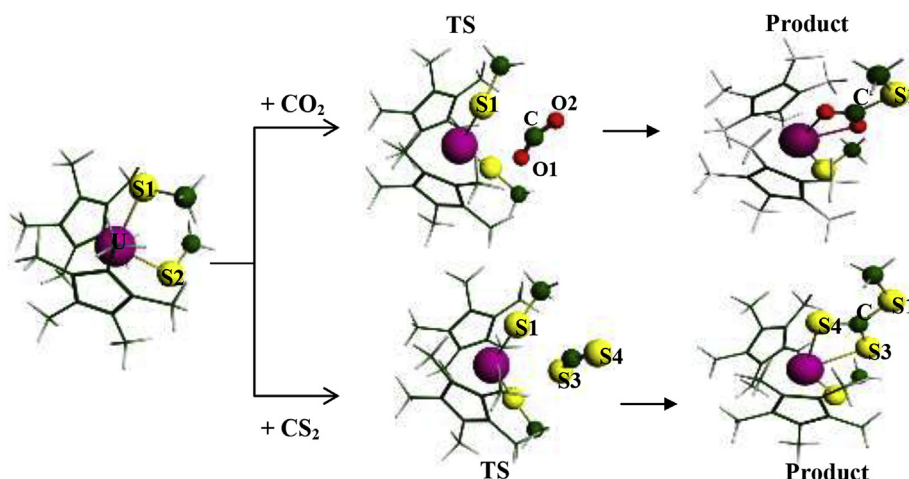


Fig. 2. Structures of the species involved in the reaction of  $[\text{U}(\text{Cp}^*)_2(\text{SMe})_2]$  and  $\text{CX}_2$  ( $\text{X} = \text{O}, \text{S}$ ).

In the following sections the characteristics of each reaction in terms of geometries, energies and NBO analysis will be detailed.

### 3.2.1. Reactivity with $\text{CS}_2$

The insertion of  $\text{CS}_2$  into the  $\text{U}-\text{S}$  bond of the  $[\text{U}(\text{Cp}^*)_2(\text{SR})_2]$  complexes proceeds first by the interaction of  $\text{CS}_2$  with the methylthiolate group  $\text{SR}$ . When the  $\text{CS}_2$  carbon atom approaches the sulfur atom of the  $\text{SR}$  group, one of the  $\text{C}-\text{S}$  bonds is elongated from 1.57 Å in free  $\text{CS}_2$  to around 1.61 Å, accompanied by a bending of the molecule of about  $156^\circ$  in the TS structures. In the meantime, the  $\text{U}-\text{S}$  bond is elongated, varying from 2.520 Å for  $\text{R} = \text{Ph}$  to 2.672 Å for  $\text{R} = \text{Me}$ , leading to the breaking of this bond. Then, the  $\text{SRC}^-$  ligand already formed coordinates to the uranium atom in the  $\eta^2-\text{SS}$  mode leading to the formation of the product  $[\text{U}(\text{Cp}^*)_2(\text{SR})(\text{S}_2\text{CSR})]$  in which  $\text{CS}_2$  is inserted into the  $\text{U}-\text{S}$  bond through the two  $\text{U}-\text{S}(\text{CS}_2)$  bonds which exhibit slightly different lengths of 2.97 and 2.91 Å. The other  $\text{U}-\text{S}$  bond lengths which are not involved in the insertion remain unchanged, around 2.766 Å.

We focus now on the reaction of  $\text{CS}_2$  with  $[\text{U}(\text{Cp}^*)_2(\text{S}^t\text{Bu})_2]$  which leads to the uranium trithiocarbonate derivative  $[\text{U}(\text{Cp}^*)_2(\text{S}^t\text{Bu})(\text{S}_2\text{CS}^t\text{Bu})]$ , the only insertion complex which was crystallographically characterized.

The computed geometry of this insertion product (Fig. 3) is in good agreement with the X-ray crystal structure. The calculated bond lengths of  $\text{U}-\text{S}_2$ ,  $\text{U}-\text{S}_3$ ,  $\text{U}-\text{S}_4$  and  $\text{U}-\text{C}_t$  are respectively 2.766, 2.956, 2.911 and 2.546 Å, whereas the experimental values are 2.643, 2.885, 2.821 and 2.490 Å, respectively. Moreover, the calculated angles are close to the experimental ones. The  $\text{S}_3-\text{U}-\text{S}_4$  bite angle is found to be  $60.4^\circ$  practically identical to the experimental value of  $62.0^\circ$ . However, the computed  $\text{U}-\text{S}$  lengths are slightly overestimated relatively to the experimental ones, as it was already observed for complex **1** (vide supra).

The IRC calculations carried out for the  $\{[\text{U}(\text{Cp}^*)_2(\text{SR})_2] + \text{CS}_2\}$  reactions (with  $\text{R} = \text{Me}, {}^t\text{Bu}, {}^i\text{Pr}, \text{Ph}$ ) showed the nonexistence of any intermediate state IM between the transition state and the reactants (or product). In all reactions for the considered spin state, the TS connects directly the reactants (at IRC backward) and the product (at IRC forward); it can be noticed that the product is always more stable than the reactants (exergonic reactions).

The energy profiles where the relative (to the reactants) enthalpies are considered and which are similar for all the  $\{[\text{U}(\text{Cp}^*)_2(\text{SR})_2] + \text{CS}_2\}$  reactions are depicted in Fig. 4.

Fig. 4(a) giving the enthalpy profile of the reaction of  $[\text{U}(\text{Cp}^*)_2(\text{SMe})_2]$  with  $\text{CS}_2$  in the gas phase, brings to light an

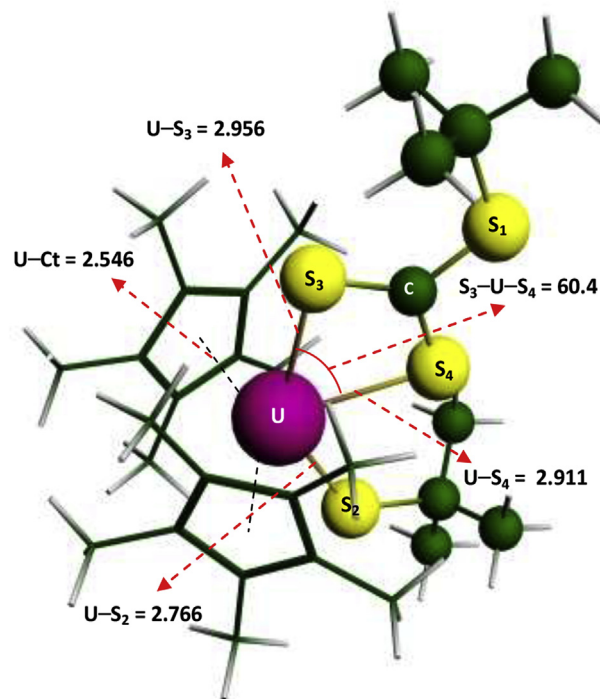


Fig. 3. Optimal geometry of the uranium trithiocarbonate complex  $[\text{U}(\text{Cp}^*)_2(\text{S}^t\text{Bu})(\text{S}_2\text{CS}^t\text{Bu})]$ .

enthalpy of activation  $\Delta H^\ddagger$  of  $23.1 \text{ kcal mol}^{-1}$  which is the lowest of the four considered reactions. The formation of the insertion product  $[\text{U}(\text{Cp}^*)_2(\text{SMe})(\text{S}_2\text{CSMe})]$  is then kinetically favored compared to the other reactions, and also thermodynamically favorable with an exothermic character of  $11.8 \text{ kcal mol}^{-1}$ . The reaction of  $[\text{U}(\text{Cp}^*)_2(\text{S}^t\text{Bu})_2]$  with  $\text{CS}_2$  seems to be the more difficult to achieve with the largest activation enthalpy ( $29.9 \text{ kcal mol}^{-1}$ ) compared to the other reactions. The exothermic character is estimated to be  $13.4$ ,  $13.2$  and  $6.2 \text{ kcal mol}^{-1}$  for  $\text{R} = {}^t\text{Bu}, {}^i\text{Pr}$  and  $\text{Ph}$  respectively indicating that the reaction of  $[\text{U}(\text{Cp}^*)_2(\text{SPh})_2]$  and  $\text{CS}_2$  is the less thermodynamically favorable in this series of reactions.

In Table 4 are reported the relative enthalpies of all stationary points (reactants, TS(s) and product) calculated in the gas phase and in toluene. As indicated in section 2, the used solvation model

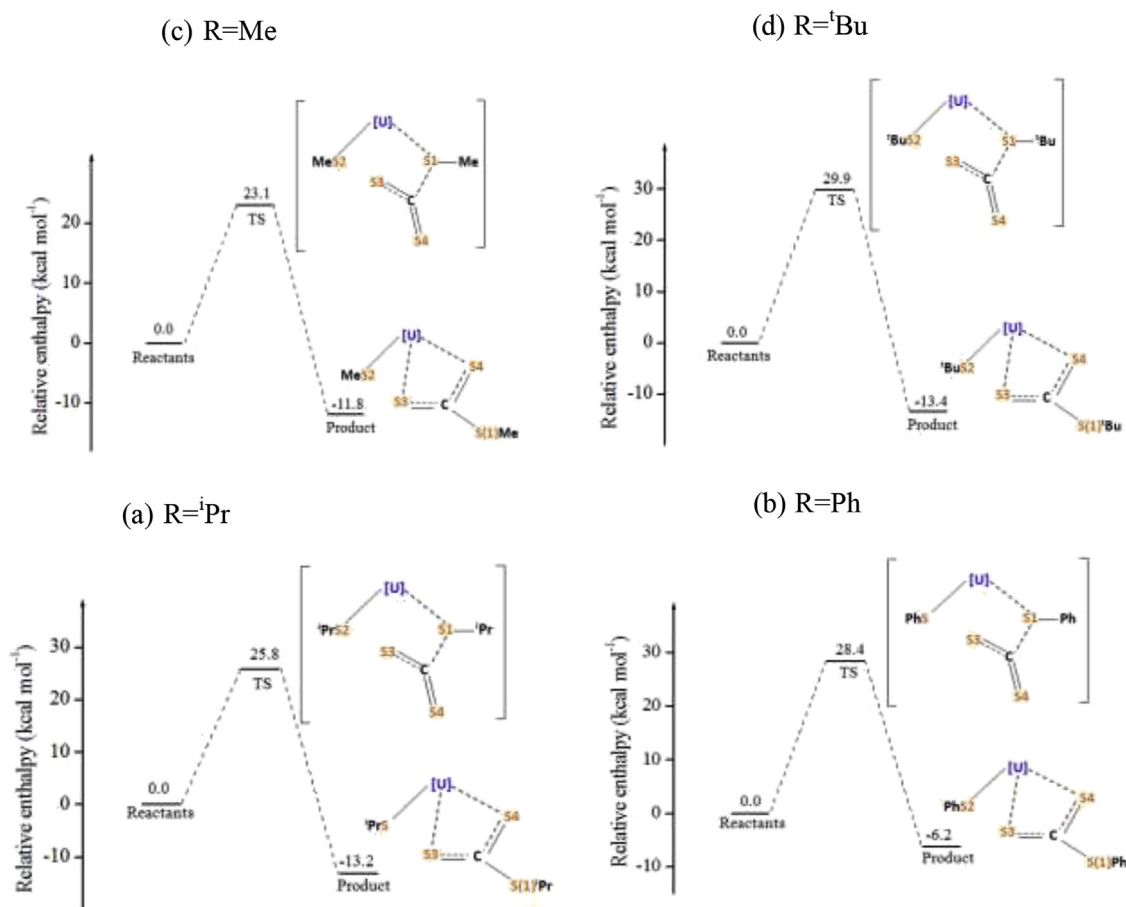


Fig. 4. Energy profiles of the  $\{[U(Cp^*)_2(SR)_2] + CS_2\}$  reactions in the gas phase.

is the SMD one the dielectric constant of toluene being equal to 2.3741. We note that the insertion reaction is more efficient in toluene since the activation energy is smaller than in the gas phase in all cases, as noted for the  $\{[U(Cp^*)_2(SMe)_2] + CS_2\}$  reaction where the reaction energy in toluene drops to  $9.2 \text{ kcal mol}^{-1}$  vs.  $23.1 \text{ kcal mol}^{-1}$  in the gas phase.

Otherwise, it is noteworthy that the activation energy  $\Delta H^\ddagger$  of the different reactions, either in the gas phase or in toluene solvent, is ranked as following:  $\Delta H^\ddagger(\text{Me}) < \Delta H^\ddagger(\text{iPr}) < \Delta H^\ddagger(\text{Ph}) < \Delta H^\ddagger(\text{tBu})$  in accordance with the steric crowding of the R group of the thiolate ligand. According to Marçalo studies [58], the steric coordination numbers of the ligands are ordered as  $\text{Me} (1.06) < \text{iPr} (1.22) < \text{Ph} (1.26) < \text{tBu} (1.50)$ . Indeed, the electrophilic attack of  $CS_2$  is favored when the SR ligand is less crowded thus facilitating the formation of a C–S bond between the C atom of the carbon disulfide and the S atom of the SR ligand. In addition, the free energy barriers ( $\Delta G^\ddagger$ ) are larger than those of activation enthalpies and

follow the same trend except for Ph and tBu complexes where the free energy barrier of the first one is slightly larger than the second one, i.e.  $39.3$  vs.  $38.9 \text{ kcal mol}^{-1}$ . However, the reaction mechanism of the  $CS_2$  insertion is performed in an identical way for the four reactions, whatever the size of the R group. The first step is characterized by a bending of  $CS_2$  molecule whereas the C ( $CS_2$ ) and  $S_1$  (SR) atoms get closer, accompanied by the lengthening of the C– $S_3$  bond and the beginning of the formation of the U– $S_3$  bond. The effective breaking of the U– $S_1$  bond comes only in the second step, when the TS barrier is overcome, accelerating thus the formation of the U– $S_3$  and U– $S_4$  bonds; it is worth noting that the formation of the U– $S_3$  bond occurs first, the formation of U– $S_4$  bond occurring by the reorientation of the  $CS_2$  molecule.

**FMO analysis of the  $\{[U(Cp^*)_2(SR)_2] + CS_2\}$  reactions.** Analysis of the frontier molecular orbitals (FMOs) of the TS of the  $\{[U(Cp^*)_2(SR)_2] + CS_2\}$  gas phase reactions has been carried out (Fig. 5). The diagram illustrates the contribution to FMOs of four

**Table 4**  
Relative Energies of Stationary Points at the B3PW91 Level of Theory: Reactants, Products and Transition States. Values in Parentheses are Relative Energies in Toluene (all Energies are in  $\text{kcal.mol}^{-1}$ ).

R	Relative energies			Reaction barrier $\Delta G^\ddagger$
	Reactants	TS Activation Energy $\Delta H^\ddagger$	Product	
Me	0 (0)	23.1 (9.2)	– 11.8 (– 24.2)	34.7
iPr	0 (0)	25.8 (12.6)	– 13.2 (– 25.5)	35.3
Ph	0 (0)	28.4 (15.7)	– 6.2 (– 16.2)	39.3
tBu	0 (0)	29.9 (18.0)	– 13.4 (– 25.1)	38.9

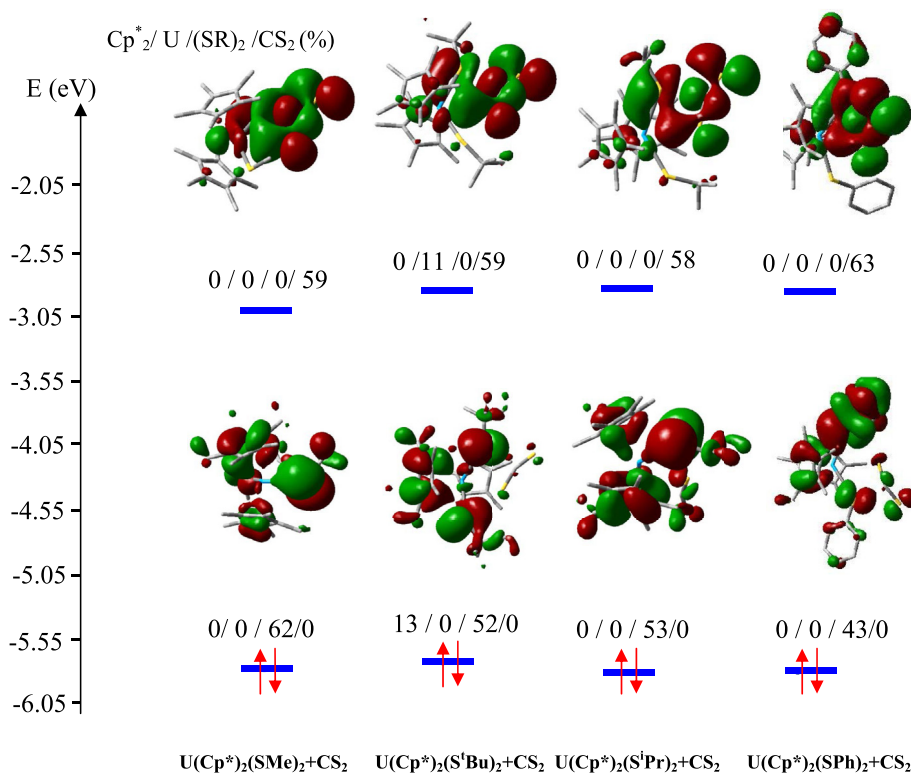


Fig. 5. FMO diagram of the transition states of the  $\{[U(Cp^*)_2(SR)_2] + CS_2\}$  reactions with the contribution of the  $(Cp^*)_2/U/(SR)_2/CS_2$  atomic orbitals to FMOs.

components: the  $(Cp^*)_2$  and  $(SR)_2$  orbitals, the U orbitals and the  $CS_2$  orbitals, as well as the FMOs energies. The HOMOs are mainly composed of the ligand  $(SR)_2$  atomic orbitals in all transition state structures, the largest value, 62%, being observed in the case of the  $\{[U(Cp^*)_2(SMe)_2] + CS_2\}$  reaction which exhibits the lowest activation barrier ( $34.7 \text{ kcal mol}^{-1}$ ) and the smallest value of 43% corresponds to the  $\{[U(Cp^*)_2(SPh)_2] + CS_2\}$  reaction which exhibits the highest activation barrier ( $39.3 \text{ kcal mol}^{-1}$ ). The other transition states exhibit intermediate compositions, 52 and 53% for the reaction of  $[U(Cp^*)_2(S^tBu)_2]$  and  $[U(Cp^*)_2(S^iPr)_2]$  with  $CS_2$  respectively, with intermediate activation barriers. The contribution of the uranium orbitals to the HOMO is negligible as well as those of  $CS_2$  whereas the  $(Cp^*)_2$  orbitals contribute with a small weight of 13% in the TS of the  $\{[U(Cp^*)_2(S^tBu)_2] + CS_2\}$  reaction. However, it is worth noting that the uranium orbitals are involved in lower energy occupied orbitals, corresponding to the bonding between the metal and the surrounding ligands.

Contrarily to the HOMOs, the LUMOs are mainly composed of  $CS_2$  orbitals and the contribution of the  $(SR)_2$  orbitals to the LUMO is negligible for the four reactions. The largest value of 63% is observed for the TS of the  $\{[U(Cp^*)_2(SPh)_2] + CS_2\}$  reaction which is the less efficient and the other values are lower but close, 59% for the  $\{[U(Cp^*)_2(SMe)_2] + CS_2\}$  and  $\{[U(Cp^*)_2(S^tBu)_2] + CS_2\}$  reactions, and 58% for the  $\{[U(Cp^*)_2(S^iPr)_2] + CS_2\}$  reaction. The Kohn–Sham HOMO–LUMO gap for the four TSs is close to 3.2 eV in average.

The reaction process has also been investigated using WBI and NPA analyses, two tools providing interesting insights into evolution of the  $CS_2$  insertion. In Table 5 are given the WBI of selected bonds involved in the insertion process, computed in the gas phase at the B3PW91 level of theory.

According to Table 5, the WBI mean values of the U– $S_1$  bond of the  $[U(Cp^*)_2(SR)_2]$  complexes and of the  $C_3$ – $S_3$  bond of  $CS_2$

decrease from 0.901 to 1.973 to 0.694 and 1.650 respectively in the transition states, in accordance with the increase of their corresponding bond lengths, showing that these bonds become weaker. On the other hand, we note the formation of a weak bond between the uranium and one of the  $CS_2$  sulfur atoms, i.e. U– $S_3$ , for which the WBI is equal to 0.484. In parallel, bonding between the carbon atom  $C_3$  of  $CS_2$  and the  $S_1$  sulfur atom of  $[U(Cp^*)_2(SR)_2]$  begins to take place, presenting a WBI equal to 0.229. The final products exhibit single bonds with WBI close to 1, except for the inserted two sulfur atoms  $S_3$  and  $S_4$  bonded to the uranium for which the bond indexes are slightly different, being equal respectively to 0.607 and 0.557. These variations are in accordance with their bond lengths, the lower WBI corresponding to the larger bond length.

The NPA results are depicted in Fig. 6 where the net charges (which are not the real ones) of relevant atoms, namely U,  $S_1$  of SR and the mean charge value of  $S_3$  and  $S_4$  of  $CS_2$  are reported, for the  $\{[U(Cp^*)_2(SMe)_2] + CS_2\}$  gas phase reaction. Thus, the NPA net charges of uranium and  $S_1$  (of SR group) atoms in  $[U(Cp^*)_2(SMe)_2]$  are around 1.90 and  $-0.36$  respectively whereas in the  $CS_2$  molecule, the carbon is negatively charged ( $-0.464$ ) and the sulfur atoms ( $S_3$  and  $S_4$ ) are positively charged (identical value of 0.231). When reaching the transition state, the NPA charge of uranium decreases revealing electronic charge transfer from ligand to uranium. At the same time the net charge of the  $S_1$  atom increases revealing a loss of electronic density. The two sulfur atoms  $S_3$  and  $S_4$  of  $CS_2$  exhibit the same trend during the different steps of the reaction, with a decrease of the NPA net charge to reach a negative value of  $-0.05$  and  $-0.02$  in the final product. These final insertion products derived from the reaction with  $CS_2$  exhibit for the uranium atom a NPA charge of 1.73, smaller than the initial charge, and for the carbon atom a charge of  $-0.604$ .

**Table 5**  
Computed WBI for the U–S<sub>1</sub> and C<sub>3</sub>–S<sub>1</sub> Bonds for the  $\{[U(Cp^*)_2(SR)_2] + CS_2\}$  reactions (R = Me, <sup>t</sup>Bu, <sup>i</sup>Pr and Ph).

	<U–S <sub>1</sub> >	<U–S <sub>2</sub> >	<C <sub>3</sub> –S <sub>3</sub> >	<C <sub>3</sub> –S <sub>4</sub> >	<C <sub>3</sub> –S <sub>1</sub> >	<U–S <sub>3</sub> >	<U–S <sub>4</sub> >
Reactants	0.901	0.900	1.973	1.973	–	–	–
TS	0.694	0.865	1.650	1.977	0.229	0.484	0.026
Product	0.034	0.868	1.313	1.340	0.941	0.607	0.557

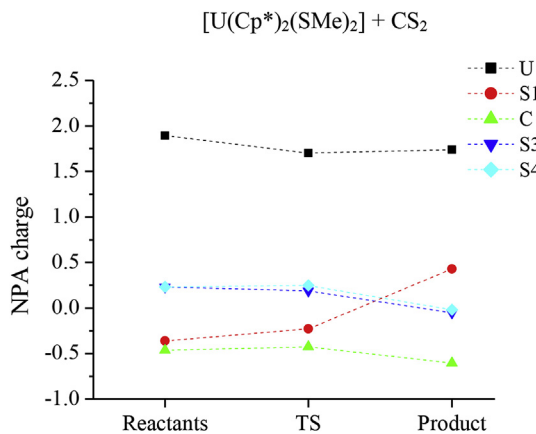


**Fig. 6.** NPA charges evolution along the  $\{[U(Cp^*)_2(SMe)_2] + CS_2\}$  reaction.

### 3.2.2. Reactivity with CO<sub>2</sub>

The mechanism of the CO<sub>2</sub> insertion reaction proceeds in a similar way than that of CS<sub>2</sub> except that the C (CO<sub>2</sub>) and S (SR) atoms get closer due to the electrostatic attraction between the positively charged carbon and the negatively charged sulfur. Thus, in the first step, the carbon dioxide interacts spontaneously with the SR group leading to the loss of the linearity of CO<sub>2</sub> reaching a bond angle around 158° in the TS(s) and the formation of a C–S bond accompanied by the lengthening of the C–O bond from 1.160 Å in free CO<sub>2</sub> to around 1.195 Å in TS(s). In parallel, the U–S bond involved in the insertion reaction is slightly elongated from ca. 2.5 Å to reach a value around 2.8 Å leading to the breaking of this bond. The insertion products  $[U(Cp^*)_2(SR)(O_2CSR)]$  are obtained by the coordination of the SRCO<sub>2</sub><sup>–</sup> ligand to the uranium atom in an η<sup>2</sup>–OO mode presenting two U–O bonds slightly different (2.47 Å and 2.52 Å).

The analysis of the CO<sub>2</sub> insertion reaction from the energy point of view is illustrated through the calculated energy profiles in terms of the relative enthalpies for the four  $\{[U(Cp^*)_2(SR)_2] + CO_2\}$  gas phase reactions which are reported in Fig. 7. As the experimental reactions of these complexes with CO<sub>2</sub> have been done in the THF solvent, the effect of this solvent (dielectric constant of 7.4257) has been considered using the SMD continuum solvation model.

In Table 6 are given the enthalpy energies of all species involved in the  $\{[U(Cp^*)_2(SR)_2] + CO_2\}$  reactions, i.e. reactants, TS and products, computed in the gas phase and in THF (used for the reaction with CO<sub>2</sub>) at the B3PW91 level of theory.

As in the case of the reaction with CS<sub>2</sub>, the  $\{[U(Cp^*)_2(SMe)_2] + CO_2\}$  reaction in the gas phase exhibits the lowest energy barrier with a value of 12.9 kcal mol<sup>–1</sup>, indicating the efficiency of this reaction which exhibits an exothermic enthalpy of –14.0 kcal mol<sup>–1</sup>. The R = <sup>i</sup>Pr group leads to the highest enthalpy barrier equal to 20.3 kcal mol<sup>–1</sup> but lower than that of the corresponding reaction with CS<sub>2</sub> which gave a barrier height equal to 25.8 kcal mol<sup>–1</sup>. The other reactions exhibit an intermediate accessible activation energy, 14.9 and 17.0 kcal mol<sup>–1</sup> for  $\{[U(Cp^*)_2(SR)_2] + CO_2\}$  reactions, with R = <sup>t</sup>Bu and Ph, respectively. As in the reactions with CS<sub>2</sub>, reactions of the bithiolate uranium

complexes with CO<sub>2</sub> depend of the steric hindrance of the R ligands, more the R steric hindrance is large more the reaction is difficult. One can see in Table 6 that the THF solvent does not affect the trend of energies but affects the values, the activation barriers and the reaction energies are much smaller than those obtained in the gas phase. From 12.9 to 20.3 kcal mol<sup>–1</sup> in the gas phase, the activation energy drops to 7.8 and 13.9 kcal mol<sup>–1</sup> respectively, the differences being estimated about 40%. Solvation facilitates the reactions.

Regarding the Wiberg Bond Indexes of the U–S bonds, the same trend as for the reaction with CS<sub>2</sub> is observed for the CO<sub>2</sub> insertion reaction. The U–S<sub>1</sub>, C<sub>3</sub>–O<sub>1</sub> and C<sub>3</sub>–O<sub>2</sub> WBI decrease along the insertion reaction, from 0.903, 1.881, 1.881 respectively for the free reactants to 0.713, 1.288, 1.380 in the transition state in the case of the  $\{[U(Cp^*)_2(SMe)_2] + CO_2\}$  reaction (Fig. 8). In the transition state, the WBI of the C–O bonds are different; one is smaller than the second indicating that the first C–O bond elongates allowing the formation of the first U–O bond, whereas the S<sub>1</sub>–C<sub>3</sub> WBI increases revealing the beginning of bonding between S<sub>1</sub> and C<sub>3</sub>. The final products exhibit single bonds, the C<sub>3</sub>–O<sub>1</sub> and C<sub>3</sub>–O<sub>2</sub> bonds have the largest WBI, close to 1.3, indicating that these bonds are very strong.

As mentioned above, the electrostatic attraction between S<sub>1</sub> and C of CO<sub>2</sub>, initiating the insertion reaction, is highlighted through the NPA charge analysis, as illustrated with the  $\{[U(Cp^*)_2(SMe)_2] + CO_2\}$  gas phase reaction (Fig. 9). In the first step (free reactants), the carbon atom of CO<sub>2</sub> possesses a positive charge (1.038) whereas the S<sub>1</sub> atom exhibits a negative charge (–0.362). We note also the charge alternation on the uranium atom (around 1.900) and oxygen atom (–0.519). From reactants to TS, the charges vary slightly whereas a noticeable charge variation occurs between TS and the product. The charge of uranium increases to reach a value around 2.170, exceeding the initial value, the same trend but in opposite direction is observed for the oxygen atom. The latter atom possesses a NPA charge of –0.519 in the free CO<sub>2</sub> molecule which reaches the value of –0.743 in the insertion product passing by the value of –0.513 in the TS.

**FMO analysis of the  $\{[U(Cp^*)_2(SR)_2] + CO_2\}$  reactions.** The FMO diagram of the TSs of the  $\{[U(Cp^*)_2(SR)_2] + CO_2\}$  gas phase reactions is displayed in Figure S16; are given the contributions to the HOMO and LUMO of the atomic orbitals of the four components: (Cp<sup>\*</sup>)<sub>2</sub> and (SR)<sub>2</sub> ligands, the uranium atom and the CO<sub>2</sub> molecule in place of CS<sub>2</sub> in the preceding reactions. According to this diagram, it is noteworthy that the (SR)<sub>2</sub> orbitals participate strongly to both HOMO and LUMO, in contrast to that observed in the insertion of CS<sub>2</sub> where strong participation is noted only to the HOMO. By comparison with the reaction with CS<sub>2</sub>, the contribution of the uranium orbitals is larger, especially in the HOMO where it reaches 20% in the case of the  $\{[U(Cp^*)_2(SMe)_2] + CS_2\}$  reaction. Also the contribution of the CO<sub>2</sub> molecule is globally negligible compared to that observed for CS<sub>2</sub> which reaches 63% in the LUMO.

### 3.2.3. Comparison of the CS<sub>2</sub> and CO<sub>2</sub> insertions into the U–S bond of the bithiolate complexes

According to the results discussed above, we note that the reactions of  $[U(Cp^*)_2(SR)_2]$  with CO<sub>2</sub> are more efficient than those with CS<sub>2</sub>. Indeed, the  $\{[U(Cp^*)_2(SMe)_2] + CS_2\}$  reaction have to overcome a high energetic barrier (23.1 kcal mol<sup>–1</sup>) compared to

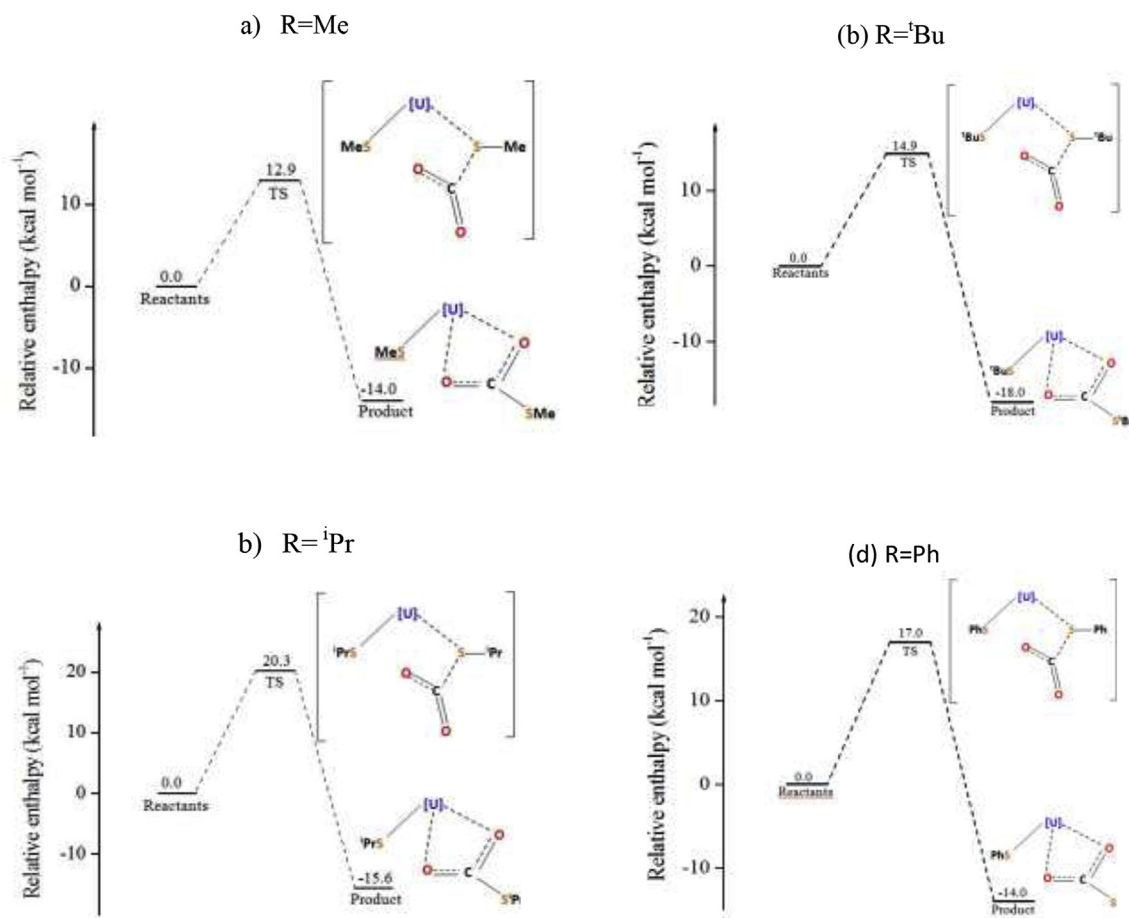


Fig. 7. Energy profiles for the  $\{[U(Cp^*)_2(SR)_2] + CO_2\}$  gasphase reactions: (a) R = Me, (b) R = <sup>t</sup>Bu (c) R = <sup>i</sup>Pr and (d) R = Ph.

Table 6

Relative Enthalpy Energies of Stationary Points at the B3PW91 Level of Theory of the  $\{[U(Cp^*)_2(SR)_2] + CO_2\}$  Reactions: Reactants, Transition States and Products (Values in Parentheses are Determined in THF, Given in kcal.mol<sup>-1</sup>).

R	Relative enthalpy energy			Reaction barrier $\Delta G^\ddagger$
	Reactants	TS Activation Energy $\Delta H^\ddagger$	Product	
Me	0 (0)	12.9 (7.8)	-14.0 (-15.7)	22.5
<sup>i</sup> Pr	0 (0)	20.3 (13.9)	-15.6 (-16.9)	29.9
Ph	0 (0)	17.0 (11.0)	-9.3 (-8.5)	26.6
<sup>t</sup> Bu	0 (0)	14.9 (7.9)	-18.0 (-19.6)	23.7

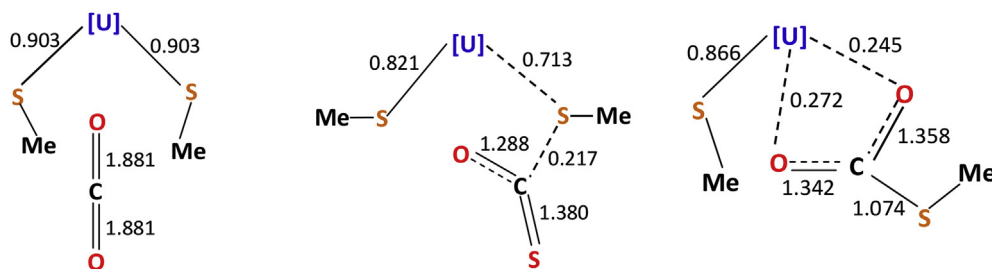


Fig. 8. Computed WBI for the  $\{[U(Cp^*)_2(SMe)_2] + CO_2\}$  gas phase reaction (from left to right, reactant, transition state and product).

the same reaction with  $CO_2$  where the barrier energy is much smaller (12.9 kcal mol<sup>-1</sup>). The reaction mechanism is identical in the two insertion reactions in view of their energy profiles. The

transition state links directly the reactant and the product without any intermediate between them. However, differences occur during the reaction processes. The NPA atomic charge distributions are

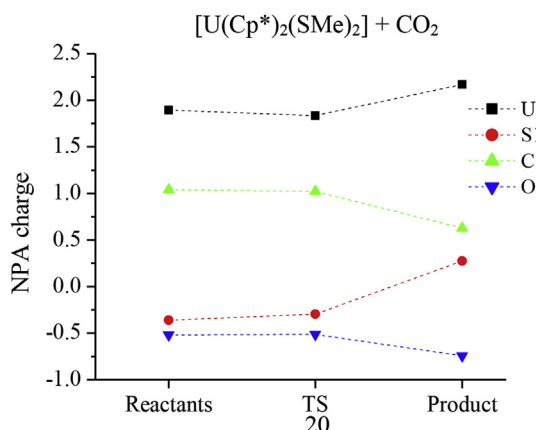


Fig. 9. NPA charges evolution along the  $[U(Cp^*)_2(SMe)_2] + CO_2$  gas phase reaction.

different for the  $CO_2$  and  $CS_2$  insertion reactions. Indeed, in addition to the oxophilic character of the uranium atom, the alternation of charges (Fig. 10) in the  $[U(Cp^*)_2(SMe)_2] + CO_2$  reaction where the C( $CO_2$ ) atom is positively charged (1.038), the S1(SR) atom is negatively charged (around  $-0.362$ ), the U atom is positively charged (around 1.870) and the O atom negatively charged (around  $-0.520$ ), promote this reaction contrarily to the reaction with  $CS_2$  where the C atom is negatively charged about  $-0.464$  and S positively charged (0.231). This charge alternation is also observed in the transition state and in the final product, the oxygen atoms acquiring a large negative charge (around  $-0.700$ ) when the uranium exhibits a charge of around 2.170. Thus, the U–O bonds exhibit a pronounced ionic character compared to the U–S bonds where the charges of the sulfur atoms are equal to  $-0.05$  and  $-0.03$ .

It seems interesting to compare the  $CS_2$  and  $CO_2$  insertion in uranium thiolate complexes to the analogous reactions of these

molecules with transition metal thiolate compounds. In the transition metal series, it seems that the  $CS_2$  insertion reaction is more favored than that of  $CO_2$ . Indeed, the reactivity of ruthenium and tungsten thiolate complexes ( $[Ru(Cp)(PPh_3)(SR)]$  and  $[W(Cp)(CO_2)(PPh_3)(SR)]$  respectively) toward  $CS_2$  and  $CO_2$  which have been explored by Shaver and co-workers [59,60] and confirmed later by Arroyo et al. [61] showed the facile insertion of  $CS_2$  into the Ru–SR bond to give the thioxanthate complexes  $[Ru(Cp)(PPh_3)(S_2CSR)]$  and into the W–SR bond to give the thioxanthate complexes  $[W(Cp)(CO_2)(S_2CSR)]$  while the reaction of  $CO_2$  with  $[W(Cp)(CO_2)(PPh_3)(SCHMe_2)]$  could not be confirmed. This reactivity is explained by the electrophilic attack by the pre-coordinated or free  $CS_2$  onto the sulfur atom of the thiolate ligand. This explanation was also reported by Arroyo for the insertion reactions of  $CS_2$  with  $[M(SR)_3(PMe_2Ph)_2]$  ( $M = Ru, Os, R = C_6F_5, C_6F_4H-4$ ). On the contrary, in the case of the uranium bithiolate complexes under study, as observed experimentally, the calculations show that the  $CO_2$  insertion into the U–S bond is more favored than the  $CS_2$  insertion regarding the activation energies. When dealing with uranium thiolate complexes it seems that the reactivity of  $CS_2$  and the  $CO_2$  which differs from that with transition metal thiolate complexes is probably due to the oxophilic character of uranium, favoring the  $CO_2$  insertion. The facile insertion reaction in the  $[U(Tp^*)_2(CH_2Ph)]$  complex of  $CO_2$  compared to that of  $CS_2$  is also noted by Ding et al. [19]; in their DFT theoretical study the uranium atom is described by a quasi-relativistic  $5f$ -in-core ECP basis. This insertion reaction is characterized by a low activation barrier equal to  $9.5 \text{ kcal mol}^{-1}$  compared to that of  $CS_2$  i.e.  $25.0 \text{ kcal mol}^{-1}$ .

#### 3.2.4. Bi-insertion with $CS_2$ and $CO_2$

The insertion reactions of the  $CO_2$  and  $CS_2$  molecules into the remaining U–S<sup>t</sup>Bu bond of  $[U(Cp^*)_2(S^tBu)(S_2CS^tBu)]$  (the product of the  $CS_2$  mono-insertion) are now investigated in gas phase using

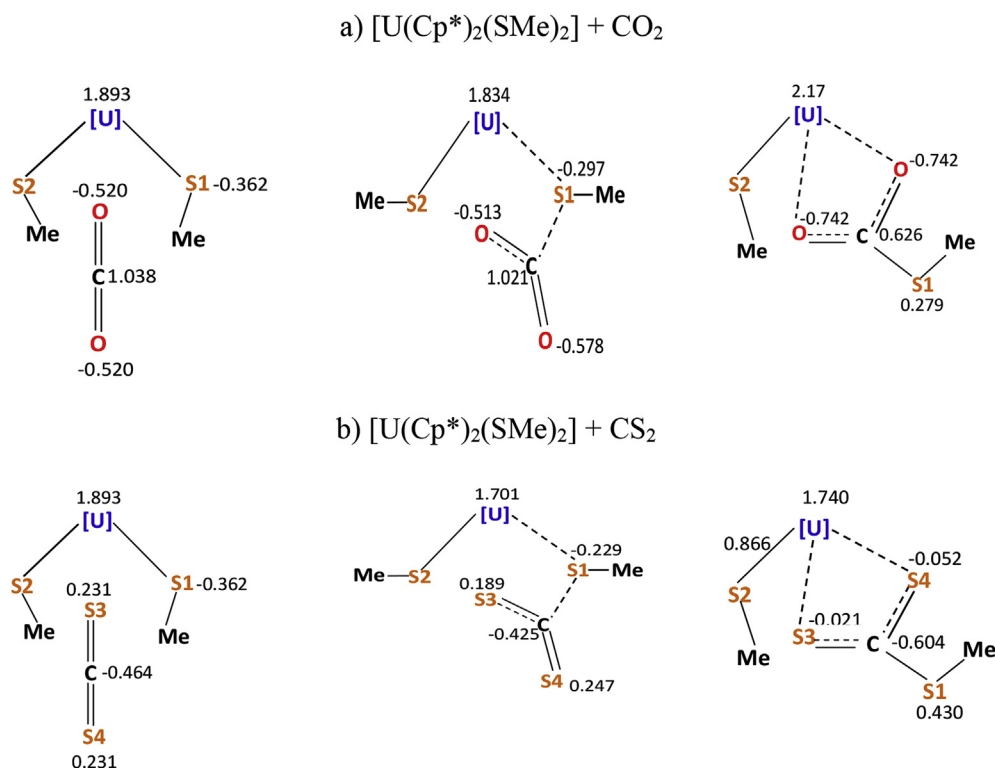


Fig. 10. NPA charge distribution on different atoms during the reactions of  $[U(Cp^*)_2(SMe)_2]$  with  $CO_2$  (a) and  $CS_2$  (b) (from left to right, reactants, TS and product).

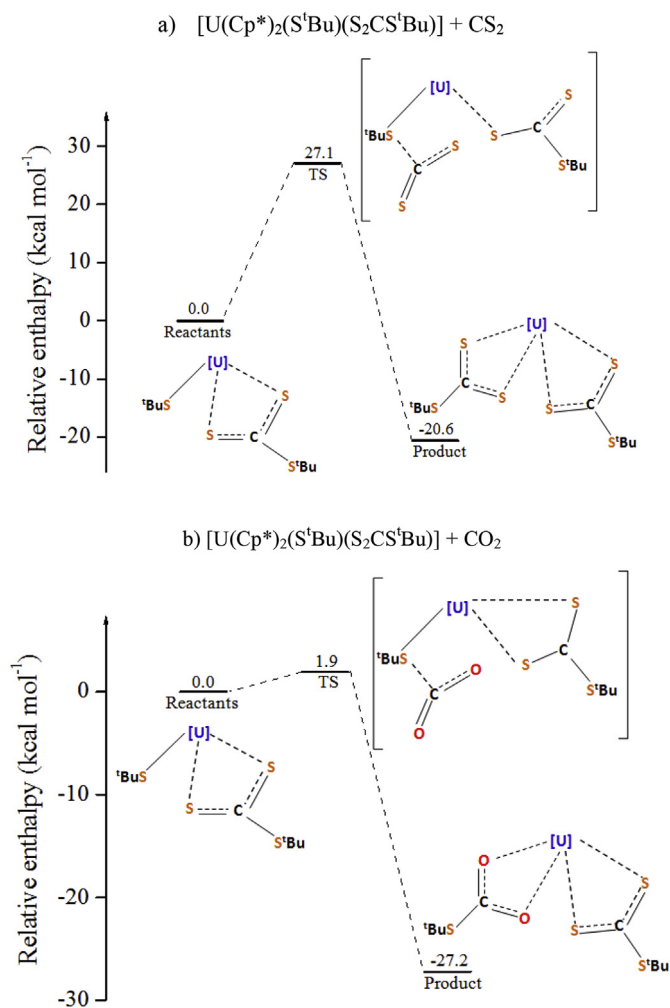


Fig. 11. Energy profiles of the bi-insertion gas phase reactions of [U(Cp\*)<sub>2</sub>(S<sup>t</sup>Bu)(S<sub>2</sub>CS<sup>t</sup>Bu)] with CS<sub>2</sub> (a) and CO<sub>2</sub> (b).

the methodology described above. The energy profile of these reactions in the gas phase is depicted in Fig. 11. As expected, due to the oxophilicity of uranium and the charge alternation between the principal atoms, the activation energy for the insertion of a second CO<sub>2</sub> molecule (1.9 kcal mol<sup>-1</sup>) is much smaller than that with CS<sub>2</sub> (27.1 kcal mol<sup>-1</sup>). Thus, the CO<sub>2</sub> insertion is more efficient, in accordance with the experimental observation where it was noted that the second insertion of CO<sub>2</sub> was much faster than the CS<sub>2</sub> insertion and was complete after 30 min under normal conditions. Thermodynamically, this reaction is also more favorable with an exothermicity of -27.2 kcal mol<sup>-1</sup>. The TS structures are similar to those observed in the mono-insertion reactions except that in the CS<sub>2</sub> bi-insertion reactions, one U–S bond of the U(S<sub>2</sub>CS<sup>t</sup>Bu) fragment is broken (U–S distance equal to 5.30 Å) but is restored at the end of the reaction (U–S distance of 3.09 Å).

#### 4. Conclusion

This work describes the structural properties of a series of bis-pentamethylcyclopentadienylbisthiolateuranium(IV) complexes [U(Cp\*)<sub>2</sub>(SR)<sub>2</sub>] (R = Me (1), <sup>t</sup>Bu (2), <sup>i</sup>Pr (3), Ph (4)) and their reactions with CO<sub>2</sub> or CS<sub>2</sub> leading to their insertion into the U–S bond, using DFT/B3PW91 computations. The optimized geometries of [U(Cp\*)<sub>2</sub>(SR)<sub>2</sub>] and the insertion derivative of 2

[U(Cp\*)<sub>2</sub>(S<sup>t</sup>Bu)(S<sub>2</sub>CS<sup>t</sup>Bu)] are found in good agreement with the X-ray crystal data. Adducts and transition states structures have been characterized and confirmed by IRC calculations. The steric and electronic factors of the R ligands play a significant role in the reactivity of the [U(Cp\*)<sub>2</sub>(SR)<sub>2</sub>] compounds; thus, it is more difficult to carry out the insertion reactions for the complex carrying the most sterically demanding S<sup>t</sup>Bu ligands (complex 2 exhibits the highest activation barrier), in accordance with the steric coordination number of the R group. With the exception of 2, all thiolate complexes promote the spontaneous carbon dioxide reduction to give the corresponding thiocarbonato complexes. Finally, the computed activation barriers of these reactions show that insertion of CO<sub>2</sub> into the U–S bond of the thiolate complexes is easier and faster than that of CS<sub>2</sub>, in agreement with the experimental observation. This distinct (best) reactivity of carbon dioxide is explained by the greatest electronegativity of O, thus allowing a good alternation of charges in the transition states, and by the well-known oxophilic character of uranium which favors initial coordination of CO<sub>2</sub> onto the metal center, before migration of the SR group. The NPA analysis shows that the insertion reaction of CO<sub>2</sub> is favored by the electrostatic attraction between the positively charged C atom and the negatively charged S atom of the SR ligand, leading to the formation of U–O bonds of more ionic character than the U–S bonds formed in the CS<sub>2</sub> insertion reaction. On the contrary, it has been pointed out that in the case of transition metal thiolate complexes the insertion of CS<sub>2</sub> is easier than the CO<sub>2</sub> insertion.

#### Note

The authors declare no competing financial interest.

#### Acknowledgments

The authors acknowledge the financial support from the Algerian Project CNEPRU n° B00L02UN150120130025. Computing facilities were provided by ASELKAM Computer Center (UMMTO, Algeria). The authors are grateful to GENCI–IDRIS and GENCI–CINES for an allocation of computing time (Grant No. 2017–2018–080649). The COST CM-1006 action is also acknowledged.

#### Appendix A. Supplementary data

Supplementary data to this article can be found online at <https://doi.org/10.1016/j.jorganchem.2019.120947>.

#### References

- [1] J.A. Labinger, J.E. Bercaw, *Nature* 417 (2002) 507–514.
- [2] H. Arakawa, M. Aresta, J.N. Armor, M.A. Barteau, E.J. Beckman, A.T. Bell, J.E. Bercaw, C. Creutz, E. Dinjus, D.A. Dixon, K. Domen, D.L. Dubois, J. Eckert, E. Fujita, D.H. Gibson, W.A. Goddard, D.W. Goodman, J. Keller, G.J. Kubas, H.H. Kunz, J.E. Lyons, L.E. Manzer, T.J. Marks, K. Morokuma, K.M. Nicholas, R. Periana, L. Que, J. Rostrup-Nielsen, W.M.H. Sachtler, L.D. Schmidt, A. Sen, G.A. Somorjai, P.C. Stair, B.R. Stults, W. Tumas, *Chem. Rev.* 101 (2001) 953–996.
- [3] J. Burdeniuc, B. Jedlicka, R.H. Crabtree, *Chem. Ber. Recueil* 130 (1997) 145–154.
- [4] B. Wayland, X. Fu, *Science* 311 (2006) 790–791.
- [5] (a) P.J. Fagan, J.M. Manriquez, E.A. Maatta, A.M. Seyam, T.J. Marks, *J. Am. Chem. Soc.* 103 (1981) 6650–6667; (b) J.M. Manriquez, P.J. Fagan, T.J. Marks, *J. Am. Chem. Soc.* 100 (1978) 3939–3941; (c) K.G. Moloy, T.J. Marks, *Inorg. Chim. Acta* 110 (1985) 127–131; (d) M. Ephritikhine, *Organometallics* 32 (2013) 2464–2488; (e) M. Ephritikhine, *Coord. Chem. Rev.* 319 (2016) 35–62.
- [6] (a) W.J. Evans, C.A. Seibel, J.W. Ziller, *Inorg. Chem.* 37 (1998) 770–776; (b) W.J. Evans, J.M. Perotti, J.C. Brady, J.W. Ziller, *J. Am. Chem. Soc.* 125 (2003) 5204–5212.

- [7] O.P. Lam, F.W. Heinemann, K. Meyer, *Angew. Chem. Int. Ed.* 50 (2011) 5965–5968.
- [8] A. Dormond, A.A. Elbouadili, C. Moise, *J. Chem. Soc., Chem. Commun.* (1984) 749–751.
- [9] (a) W.J. Evans, J.R. Walensky, J.W. Ziller, A.L. Rheingold, *Organometallics* 28 (2009) 3350–3357;  
(b) W.J. Evans, N.A. Siladke, J.W. Ziller, *Chem. Eur. J.* (2010) 796–797.
- [10] (a) K.C. Jantunen, C.J. Burns, I. Castro-Rodríguez, R.E. Da Re, J.T. Golden, D.E. Morris, B.L. Scott, F.L. Taw, J.L. Kiplinger, *Organometallics* 23 (2004) 4682–4692;  
(b) J.A. Pool, B.L. Scott, J.L. Kiplinger, *J. Am. Chem. Soc.* 127 (2005) 1338–1339.
- [11] (a) J.G. Brennan, R.A. Andersen, A. Zalkin, *Inorg. Chem.* 25 (1986) 1756–1760;  
(b) I. Castro-Rodríguez, H. Nakai, L.N. Zakharov, A. L. Rheingold, K. Meyer, *Science* 305 (2004) 1757–1759;  
(c) J.G. Brennan, R.A. Andersen, A. Zalkin, *Inorg. Chem.* 25 (1986) 1761–1765.
- [12] (a) J.C. Berthet, J.F. Le Maréchal, M. Nierlich, M. Lance, J. Vigner, M. Ephritikhine, *J. Organomet. Chem.* 408 (1991) 335–341;  
(b) I. Castro-Rodríguez, K. Meyer, *J. Am. Chem. Soc.* 127 (2005) 11242–11243.
- [13] S.M. Mansell, N. Kaltsoyannis, P.L. Arnold, *J. Am. Chem. Soc.* 133 (2011) 9036–9051.
- [14] (a) O.T. Summerscales, F.G.N. Cloke, P.B. Hitchcock, J.C. Green, N. Hazari, *Science* 311 (2006) 829–831;  
(b) O.T. Summerscales, F.G.N. Cloke, P.B. Hitchcock, J.C. Green, N. Hazari, *J. Am. Chem. Soc.* 128 (2006) 9602–9603;  
(c) P.L. Arnold, Z.B. Turner, R.M. Bellabarda, R.P. Tooze, *Chem* 2 (2011) 77–79;  
(d) B.M. Gardner, J.C. Stewart, A.L. Davis, J. McMaster, W. Lewis, A.J. Blake, S.T. Little, *Proc. Natl. Acad. Sci. U.S.A.* 109 (2012) 9265–9270;  
(e) A.S. Frey, F.G.N. Cloke, P.B. Hitchcock, I.J. Day, J.C. Green, G. Aitken, *J. Am. Chem. Soc.* 130 (2008) 13816–13817;  
(f) G.J. Brennan, R.A. Andersen, J.L. Robbins, *J. Am. Chem. Soc.* 108 (1986) 335–336.
- [15] (a) P. Russel, P.J. Scott, *J. Am. Chem. Soc.* 120 (1998) 1070–1071;  
(b) F.G.N. Cloke, P.B. Hitchcock, *J. Am. Chem. Soc.* 124 (2002) 9352–9353.
- [16] N. Tsoureas, O.T. Summerscales, F.G.N. Cloke, S.M. Roe, *Organometallics* 32 (2013) 1353–1362.
- [17] (a) V. Mougél, C. Camp, J. Pécaut, C. Copéret, L. Maron, C.E. Kefalidis, M. Mazzanti, *Angew. Chem. Int. Ed.* 51 (2012) 12280–12284;  
(b) O. Cooper, C. Camp, J. Pécaut, C.E. Kefalidis, L. Maron, S. Gambarelli, M. Mazzanti, *J. Am. Chem. Soc.* 136 (2014) 6716–6723.
- [18] (a) O.T. Summerscales, A.S. Frey, F.G.N. Cloke, P.B. Hitchcock, *Chem. Commun.* (2009) 198–200;  
(b) E.M. Matson, A.T. Breshears, J.J. Kiernicki, B.S. Newell, P.E. Fanwick, M.P. Shores, J.R. Walensky, S.C. Bart, *Inorg. Chem.* 53 (2014) 12977–12985.
- [19] W. Ding, W. Fang, Z. Chai, D. Wang, *J. Chem. Theory Comput.* 8 (2012) 3605–3617.
- [20] L. Castro, L. Maron, *Chem. Eur. J.* 18 (2012) 6610–6615.
- [21] C.J. Inman, A.S.P. Frey, A.F.R. Kilpatrick, F.G.N. Cloke, S.M. Roe, *Organometallics* 36 (2017) 4539–4545.
- [22] J.M. Berg, R.H. Holm 4, Interscience, New York, 1982.
- [23] D. Coucouvanis, *Ace. Chem. Res.* 24 (1991) 1–8.
- [24] B.C. Wiegand, C.M. Friend, *Chem. Rev.* 92 (1992) 491–496.
- [25] I. Santos, N. Marques, A. Pires de Matos, *Inorg. Chim. Acta* 139 (1987) 89–90.
- [26] Z. Lin, C.P. Brock, T.J. Marks, *Inorg. Chim. Acta* 141 (1988) 145–149.
- [27] K. Tatsumi, I. Matsubara, Y. Inoue, A. Nakamura, R.E. Cramer, G.J. Tagoshi, J.A. Golen, J.W. Gilje, *Inorg. Chem.* 29 (1990) 4928–4938.
- [28] (a) S.D. Stults, R.A. Andersen, A. Zalkin, *Organometallics* 9 (1990) 1623–1629;  
(b) A. Domingos, A. Pires de Matos, I. Santos, *Polyhedron* 11 (1992) 1601–1606.
- [29] D.L. Clark, M.M. Miller, J.G. Watkin, *Inorg. Chem.* 32 (1993) 772–774.
- [30] E.M. Matson, P.E. Fanwick, S.C. Bart, *Organometallics* 30 (2011) 5753–5762.
- [31] (a) P.C. Leverd, T. Arliguie, M. Lance, M. Nierlich, J. Vigner, M. Ephritikhine, *J. Chem. Soc. Dalton Trans.* (1994) 501–504;  
(b) P.C. Leverd, M. Ephritikhine, M. Lance, J. Vigner, M. Nierlich, *J. Organomet. Chem.* 507 (1996) 229–237.
- [32] C. Lescop, T. Arliguie, M. Lance, M. Nierlich, M. Ephritikhine, *J. Organomet. Chem.* 580 (1999) 137–144.
- [33] F.T. Edlmann, in: G. Wilkinson, F.G.A. Stone, E.W. Abel (Eds.), *Comprehensive Organometallic Chemistry*, vol. 4, Pergamon, Oxford, 1995, pp. 11–130.
- [34] K.B. Wiberg, *Tetrahedron* 24 (1968) 1083–1096.
- [35] A.E. Reed, R.B. Weinstock, F. Weinhold, *J. Chem. Phys.* 83 (1985) 735–746.
- [36] Gaussian 09, Revision D.01 M.J. Frisch, G.W. Trucks, H.B. Schlegel, G.E. Scuseria, M.A. Robb, J.R. Cheeseman, G. Scalmani, V. Barone, B. Mennucci, G.A. Petersson, H. Nakatsuji, M. Caricato, X. Li, H.P. Hratchian, A.F. Izmaylov, J. Bloino, G. Zheng, J.L. Sonnenberg, M. Hada, M. Ehara, K. Toyota, R. Fukuda, J. Hasegawa, M. Ishida, T. Nakajima, Y. Honda, O. Kitao, H. Nakai, T. Vreven, J.A. Montgomery, J.E. Peralta, F. Ogliaro, M. Bearpark, J.J. Heyd, E. Brothers, K.N. Kudin, V.N. Staroverov, R. Kobayashi, J. Normand, K. Raghavachari, A. Rendell, J.C. Burant, S.S. Iyengar, J. Tomasi, M. Cossi, N. Rega, J.M. Millam, M. Klene, J.E. Knox, J.B. Cross, V. Bakken, C. Adamo, J. Jaramillo, R. Gomperts, R.E. Stratmann, O. Yazyev, A.J. Austin, R. Cammi, C. Pomelli, J.W. Ochterski, R.L. Martin, K. Morokuma, V.G. Zakrzewski, G.A. Voth, P. Salvador, J.J. Dannenberg, S. Dapprich, A.D. Daniels, O. Farkas, J.B. Foresman, J.V. Ortiz, J. Cioslowski, D.J. Fox, Gaussian Inc., Wallingford CT, 2013.
- [37] A.D. Becke, *J. Chem. Phys.* 98 (1993) 5648–5652.
- [38] (a) J.P. Perdew, Y. Wang, *Phys. Rev. B* 45 (1992) 13244–13249;  
(b) K. Burke, J.P. Perdew, W. Yang, in: J.F. Dobson, G. Vignale, M.P. Das (Eds.), *Electronic Density Functional Theory: Recent Progress and New Directions*, Springer, Heidelberg, 1998.
- [39] L. Castro, S.C. Bart, O.P. Lam, K. Meyer, L. Maron, *Organometallics* 29 (2010) 5504–5510.
- [40] (a) A. Moritz, M. Dolg, *Chem. Phys.* 337 (2007) 48–54;  
(b) A. Moritz, X.Y. Cao, M. Dolg, *Theor. Chem. Acc.* 118 (2007) 845–854;  
(c) M. Dolg, H. Stoll, H. Preuss, *J. Chem. Phys.* 90 (1989) 1730–1734;  
(d) X. Cao, M. Dolg, *J. Chem. Phys.* 115 (2001) 7348–7355.
- [41] (a) M. Dolg, H. Stoll, A. Savin, H. Preuss, *Theor. Chim. Acta* 75 (1989) 173–194;  
(b) M. Dolg, H. Stoll, H. Preuss, *Theor. Chim. Acta* 85 (1993) 441–450.
- [42] A. Bergner, M. Dolg, W. Kuechle, H. Stoll, H. Preuss, *Mol. Phys.* 80 (1993) 1431–1441.
- [43] A.W. Ehlers, M. Bohme, S. Dapprich, A. Gobbi, A. Hollwarth, V. Jonas, K.F. Kohler, R. Stegmann, A. Veldkamp, G.A. Frenking, *Chem. Phys. Lett.* 208 (1993) 111–114.
- [44] A.V. Marenich, C.J. Cramer, D.G. Truhlar, *J. Phys. Chem. B* 113 (2009) 6378–6396.
- [45] (a) W.J. Hehre, R. Ditchfield, J.A. Pople, *J. Chem. Phys.* 56 (1972) 2257–2261;  
(b) P.C. Hariharan, J.A. Pople, *Theor. Chim. Acta* 28 (1973) 213–222.
- [46] (a) L. Castro, A. Yahia, L. Maron, *Chim. Chim. Acta* 13 (2010) 870–875;  
(b) L. Castro, A. Yahia, L. Maron, *ChemPhysChem* 11 (2010) 990–994.
- [47] V. Mougél, C. Camp, J. Pécaut, C. Copéret, L. Maron, C.E. Kefalidis, M. Mazzanti, *Angew. Chem. Int. Ed.* 51 (2012) 12280–12284.
- [48] S. Labouille, F. Nief, L. Maron, *J. Phys. Chem.* 115 (2011) 8295–8301.
- [49] L. Castro, C.E. Kefalidis, D. McKay, S. Essafi, L. Perrin, L. Maron, *Dalton Trans.* 43 (2014) 12124–12134.
- [50] L. Castro, S. Labouille, D.R. Kindra, J.W. Ziller, F. Nief, W.J. Evans, L. Maron, *Chem. Eur. J.* 18 (2012) 7886–7895.
- [51] (a) C. Gonzalez, H.B. Schlegel, *J. Chem. Phys.* 90 (1989) 2154–2161;  
(b) C. Gonzalez, H.B. Schlegel, *J. Phys. Chem.* 94 (1990) 5523–5527.
- [52] A.V. Marenich, C.J. Cramer, D.G. Truhlar, *J. Phys. Chem. B* 113 (2009) 6378–6396.
- [53] E. Van Lenthe, J.G. Snijders, E.J. Baerends, *J. Chem. Phys.* 105 (1996) 6505–6516.
- [54] H. Xiao, J. Li, *Chin. J. Struct. Chem.* 27 (2008) 967–974.
- [55] J.T. Lyon, L. Andrews, P. Malmqvist, B.O. Roos, T. Yang, B.E. Bursten, *Inorg. Chem.* 46 (2007) 4917–4925.
- [56] L. Gagliardi, B.O. Roos, P. Malmqvist, J.M. Dyke, *J. Phys. Chem. A* 105 (2001) 10602–10606.
- [57] (a) R.S. Mulliken, *J. Chem. Phys.* 23 (1955) 1833–1840, 2338–2342;  
(b) R.S. Mulliken, W.C. Ermler, *Diatom. Molecules: Results of Ab Initio Calculations*, Academic, New York, 1977, pp. 33–38.
- [58] J. Marçalo, A. Pires De Matos, *Polyhedron* 8 (1989) 2431–2437.
- [59] A. Shaver, P.Y. Plouffe, P. Bird, E. Livingstone, *Inorg. Chem.* 29 (1990) 1826–1830.
- [60] A. Shaver, B.S. Lum, P. Bird, K. Arnold, *Inorg. Chem.* 28 (1989) 1900–1904.
- [61] M. Arroyo, S. Bernès, J. Cerón, J. Rius, H. Torrens, *Inorg. Chem.* 43 (2004) 986–992.